



This is a repository copy of *Highly porous polycaprolactone microspheres for skeletal repair promote a mature bone cell phenotype in vitro.*

White Rose Research Online URL for this paper:

<https://eprints.whiterose.ac.uk/218660/>

Version: Published Version

---

**Article:**

Paterson, T.E. [orcid.org/0000-0002-2951-115X](https://orcid.org/0000-0002-2951-115X), Owen, R. [orcid.org/0000-0003-1961-0733](https://orcid.org/0000-0003-1961-0733), Sherborne, C. et al. (5 more authors) (2024) Highly porous polycaprolactone microspheres for skeletal repair promote a mature bone cell phenotype in vitro. *Journal of Materials Chemistry B: Materials for biology and medicine*, 12 (45). pp. 11746-11758. ISSN 2050-750X

<https://doi.org/10.1039/d4tb01532k>

---

**Reuse**

This article is distributed under the terms of the Creative Commons Attribution (CC BY) licence. This licence allows you to distribute, remix, tweak, and build upon the work, even commercially, as long as you credit the authors for the original work. More information and the full terms of the licence here:

<https://creativecommons.org/licenses/>

**Takedown**

If you consider content in White Rose Research Online to be in breach of UK law, please notify us by emailing [eprints@whiterose.ac.uk](mailto:eprints@whiterose.ac.uk) including the URL of the record and the reason for the withdrawal request.










[eprints@whiterose.ac.uk](mailto:eprints@whiterose.ac.uk)  
<https://eprints.whiterose.ac.uk/>



Cite this: DOI: 10.1039/d4tb01532k

# Highly porous polycaprolactone microspheres for skeletal repair promote a mature bone cell phenotype *in vitro*†

Thomas E. Paterson,  ‡<sup>abc</sup> Robert Owen,  ‡<sup>\*d</sup> Colin Sherborne,<sup>a</sup>  
Hossein Bahmaee,  <sup>ac</sup> Amy L. Harding,  <sup>b</sup> Nicola H. Green,  <sup>ac</sup>  
Gwendolen C. Reilly  <sup>\*ac</sup> and Frederik Claeysens  <sup>\*a</sup>

Improving our ability to treat skeletal defects is a critical medical challenge that necessitates the development of new biomaterials. One promising approach involves the use of degradable polymer microparticles with an interconnected internal porosity. Here, we employed a double emulsion to generate such round microparticles (also known as microspheres) from a polycaprolactone-based polymerised high internal phase emulsion (polyHIPE). These microspheres effectively supported the growth of mesenchymal progenitors over a 30-day period, and when maintained in osteogenic media, cells deposited a bone-like extracellular matrix, as determined by histological staining for calcium and collagen. Interestingly, cells with an osteocyte-like morphology were observed within the core of the microspheres indicating the role of a physical environment comparable to native bone for this phenotype to occur. At later timepoints, these cultures had significantly increased mRNA expression of the osteocyte-specific markers dentin matrix phosphoprotein-1 (Dmp-1) and sclerostin, with sclerostin also observed at the protein level. Cells pre-cultured on porous microspheres exhibited enhanced survival rates compared to those pre-cultured on non-porous counterparts when injected. Cells precultured on both porous and non-porous microspheres promoted angiogenesis in a chorioallantoic membrane (CAM) assay. In summary, the polycaprolactone polyHIPE microspheres developed in this study exhibit significant promise as an alternative to traditional synthetic bone graft substitutes, offering a conducive environment for cell growth and differentiation, with the potential for better clinical outcomes in bone repair and regeneration.

Received 12th July 2024,  
Accepted 7th October 2024

DOI: 10.1039/d4tb01532k

rsc.li/materials-b

## Introduction

Bone is the second most transplanted tissue in the world after blood with over 2 million bone graft procedures performed each year worldwide. With global increases in life expectancy and population, there is an ever growing need to improve our ability to treat skeletal defects and augment bone.<sup>1</sup> Whilst auto- and allografts remain the gold standard, synthetic bone graft substitutes are also commonly used to meet demand.<sup>2</sup> These are typically bioceramic-based, and whilst partially successful in clinical use, complications occur due to poor mechanical

properties and inappropriate resorption rates.<sup>3,4</sup> Bone tissue engineering has the potential to help address this healthcare need by providing scaffolds that act as improved synthetic bone graft substitutes.<sup>5</sup> Scaffolds have been fabricated by a vast range of manufacturing methods, ranging from solvent casting/particulate leaching to electrospinning and additive manufacturing.<sup>6</sup> However, to meet clinical needs and facilitate translation, these products must ultimately be manufactured through a scalable process and provided in an accessible, easy-to-use form. Ideally, they should be administrable surgically in a manner analogous to existing bone graft substitute products, such as granules or microparticles.

To successfully facilitate bone regeneration, biomaterials implanted into the defect site need to integrate with the surrounding tissues and undergo timely cellularisation and vascularisation.<sup>7</sup> Microparticle technologies have attracted increased research attention in recent years within bone tissue engineering due to their ability to act as bulk scaffolds and drug-delivery vehicles.<sup>8,9</sup> Moreover, their ability to achieve high packing densities may enhance tissue integration through superior interfacing with defect edges compared to monolithic scaffolds.<sup>10</sup> However, to ensure sufficient

<sup>a</sup> Department of Materials Science and Engineering, The Kroto Research Institute, University of Sheffield, Sheffield, UK. E-mail: g.reilly@sheffield.ac.uk, f.claeysens@sheffield.ac.uk

<sup>b</sup> School of Clinical Dentistry, University of Sheffield, Sheffield, UK

<sup>c</sup> INSIGNEO Institute for in silico Medicine, University of Sheffield, Sheffield, UK

<sup>d</sup> School of Pharmacy, University of Nottingham Biodiscovery Institute, University of Nottingham, Nottingham, UK. E-mail: robert.owen@nottingham.ac.uk

† Electronic supplementary information (ESI) available. See DOI: <https://doi.org/10.1039/d4tb01532k>

‡ Joint first authors.



free volume remains in the filled defect for tissue and vascular ingrowth, there must also be interconnected porosity within and between the microparticles. Ideally, microparticles should be made from a biodegradable material that resorbs at a rate comparable to new tissue formation to allow full remodelling of the defect site.<sup>11</sup> Microparticle-based systems that permit the possibility of being used as both acellular void fillers and as a carrier to deliver cells therapeutically to promote survival within the defect site will have the broadest application in skeletal repair.<sup>8</sup>

Polymer microparticles for regenerative medicine have been produced by a wide range of manufacturing techniques, including emulsification *via* both traditional and microfluidic approaches, electrospraying, phase separation and grinding.<sup>12,13</sup> Microparticles can either be solid or porous, with the former confining cell attachment and tissue formation to the surface. Whilst these successfully fill defect voids and permit osteogenesis in the spaces between particles, histological analysis reveals entrapped polymer within the new tissue that impedes full bone remodelling until degraded.<sup>4,14,15</sup> Porous polymer microparticles, such as those used for cell expansion, permit cell ingrowth and allow more continuous neo-tissue formation.<sup>16,17</sup> Microparticles that are produced in a spherical form are often classified as microspheres. Herein, we will use the term microspheres for round microparticles.

Highly porous scaffolds for bone tissue engineering and 3D cell culture substrates, made from polymerised high internal phase emulsion (polyHIPE)-based materials, have attracted increasing research interest in recent years. This is due to the high porosity, interconnectivity, and tunability offered by the process.<sup>18</sup> By using a photocurable pre-polymer for the continuous phase of the emulsion with an internal phase volume above 74%, a highly interconnected, highly porous polymer is produced when polymerised and the internal phase removed.<sup>19</sup> For *in vitro* bone cell culture, non-degradable polyHIPES have been fabricated into scaffolds using additive manufacturing,<sup>20,21</sup> soft lithography,<sup>22</sup> and porogen leaching,<sup>23</sup> as well as being formed into microspheres using double emulsion<sup>24</sup> and microfluidic techniques.<sup>25</sup> We recently developed and characterised the material properties (structure (NMR), molecular weight (GPC), mechanical properties, density, porosity, degradation) of a biodegradable, photocurable polycaprolactone (PCL)-based polyHIPE<sup>26</sup> that has been shown to support bone growth both *in vitro*<sup>27,28</sup> and *in vivo*<sup>29</sup> in 3D printed scaffolds. Whilst other non-degradable<sup>24</sup> and degradable<sup>30</sup> polyHIPE materials have been fabricated into porous polymer microspheres through a double emulsion approach, this has not yet been achieved using a biodegradable PCL-based polyHIPE.

Here, we present a route to creating PCL-based, highly porous, polyHIPE microspheres for bone tissue engineering applications, assessing their degradability, ability to support bone cell cultures over extended time periods, and suitability for promoting injected cell survival.

## Results and discussion

This study aimed to assess the amenability of polycaprolactone (PCL)-based polyHIPE materials to porous microsphere

manufacture and their suitability for skeletal repair applications. Whilst porous PCL microspheres have been made previously by phase separation and emulsion/solvent evaporation, these approaches cannot achieve the same porosity as high internal phase emulsion approaches.<sup>31,32</sup> Porous polyHIPE microspheres have previously been generated from both non-degradable and degradable monomers; however, neither of these approaches directly supported the adherence of mammalian cells and required plasma modification prior to cell culture,<sup>24</sup> or only affected cells indirectly through controlled release of growth factors<sup>30</sup> rather than by acting as a substrate for cell culture.

### PCL polyHIPE microspheres can be produced using double emulsion templating

Using a water-in-oil-in-water (w/o/w) double emulsion, highly porous PCL polyHIPE microspheres were fabricated ranging from 25 to 1000  $\mu\text{m}$  diameter. After sieving, microspheres below 500  $\mu\text{m}$  were retained for investigation, with a mean and median diameter of  $157.6 \pm 132.3 \mu\text{m}$  and 93.2  $\mu\text{m}$ , respectively (Fig. 1A). Morphology of the microspheres was assessed using CellProfiler by segmenting particles as primary objects and measuring shape parameters. They were slightly elliptical, with a mean eccentricity (perfect circle: 0.0) of  $0.5 \pm 0.2$ , likely due to the forces exerted during mixing in the second emulsion prior to photopolymerisation (Fig. 1B). The classical interconnected polyHIPE microporosity was retained within the microspheres (Fig. 1C). Rapid characterisation of biomaterial morphology using computer vision (digitizing tasks humans do by sight) is emerging as a powerful tool.<sup>33</sup> Here, we used 'Pore D<sup>2</sup>', an open-source deep learning tool developed for extracting morphological information from polyHIPE SEM images<sup>34</sup> to quantify pore and interconnect size, calculating a mean and median pore diameter of  $23.5 \pm 14.5 \mu\text{m}$  and 19.9  $\mu\text{m}$ , respectively (Fig. 1D), and a mean and median pore interconnect diameter of  $6.3 \pm 3.5 \mu\text{m}$  and 5.9  $\mu\text{m}$ , respectively (Fig. 1E).

Over a 60-day period, microspheres underwent significant mass loss in both standard aqueous ( $23.3 \pm 15.3\%$ ,  $p < 0.05$ ) and accelerated basic (pH 13) ( $82.2 \pm 7.0\%$ ,  $p < 0.01$ ) conditions (Fig. 1F). PCL degrades by hydrolysis of the ester linkages in the polymer backbone, with  $\text{OH}^-$  ions present in basic conditions catalysing this process.<sup>35</sup> Previous degradation studies on non-polyHIPE (solid) variants of this PCL-M showed a linear degradation profile that could be tuned through variation of the degree of methacrylation due to its influence on crosslink density.<sup>36</sup> Degradation rates observed here were only marginally slower than the previous study despite using 0.1 M sodium hydroxide (NaOH) rather than 5 M, demonstrating how increasing surface area accelerates hydrolysis. Whilst an advantage of PCL over other synthetic polymers such as PLA is its slower degradation rate reduces local accumulation of inflammatory, acidic byproducts, future work will need to identify a PCL-M formulation that degrades at an appropriate rate *in vivo* in a bone defect to allow tissue healing whilst avoiding inflammation.<sup>37</sup>

The double emulsion (w/o/w) microsphere fabrication technique used here produced a wide distribution of particle sizes and some variation in morphology consistent with other



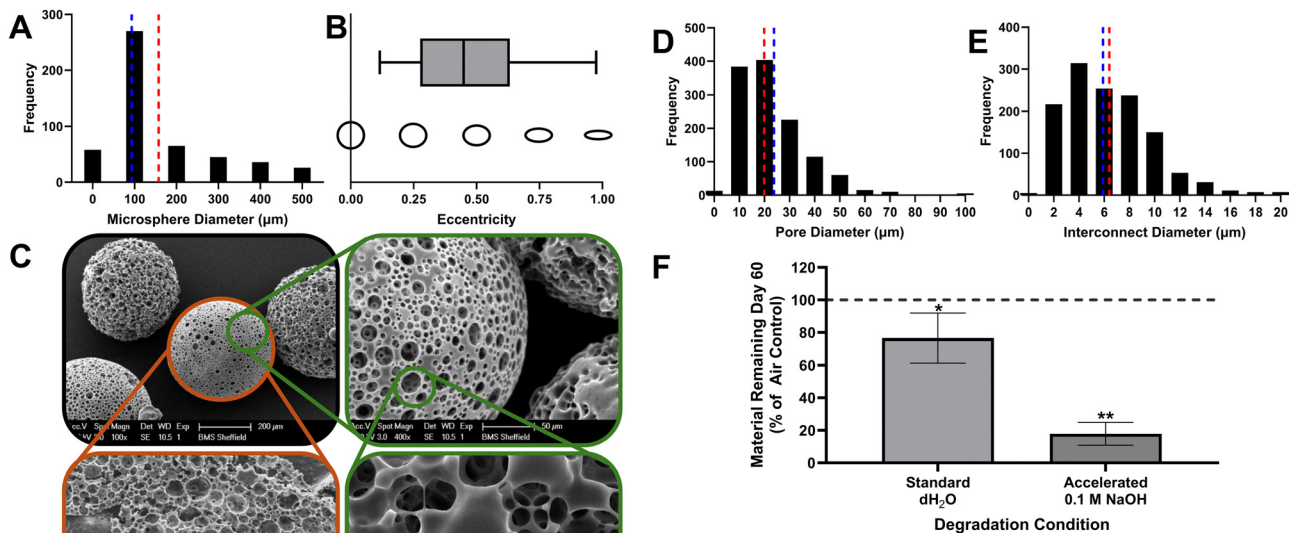


**Fig. 1** PCL polyHIPE microspheres formed by w/o/w emulsion templating. (A) Size distribution of microsphere diameters (mean (red): 157.6  $\mu\text{m}$ , median (blue): 93.2  $\mu\text{m}$ ,  $n = 500$ ). (B) Min–max eccentricity of microspheres with example circles for each value below (perfect circle: 0, most elliptical: 0.95). Microspheres were slightly elliptical. (C) Representative SEM images of PCL polyHIPE microsphere morphology at increasing magnification (green) and of a bisected microsphere (red). (D) Size distribution of polyHIPE micropores (mean (red): 23.5  $\mu\text{m}$ , median (blue): 19.9  $\mu\text{m}$ ,  $n = 1244$ ). (E) Size distribution of polyHIPE interconnects (mean (red): 6.3  $\mu\text{m}$ , median (blue): 5.9  $\mu\text{m}$ ,  $n = 1294$ ). (F) Degradation of the PCL microspheres resulted in significant mass loss in both standard (23.3%) and accelerated conditions (82.2%) over a 60-day period.

emulsion-based studies.<sup>38,39</sup> Whilst this can be reduced through sieving, recent studies demonstrate that microfluidic approaches would be a more efficient technology for producing monodisperse, uniform microsphere populations in the future<sup>40,41</sup> as it is a route to scalable production.<sup>42</sup> However, whether monodisperse microsphere diameters are desirable from a clinical perspective is not established. Achieving a better clinical outcome is partly dependent on successful microsphere integration with the surrounding tissue, which can be improved by maximising microsphere contact with the defect edges. The maximum theoretical packing density for equal spheres in a cubic volume is 74%,<sup>43</sup> whereas a polydisperse range of sphere sizes achieves a higher theoretical packing density due to smaller spheres filling voids left between larger spheres. Therefore, it may be the case that a densely packed, polydisperse, porous microsphere population is preferable to a monodisperse counterpart due to its ability to achieve better edge integration whilst retaining an interconnected microporous network.

### Osteogenic culture conditions promote cell infiltration into the microporous network

Human embryonic stem cell-derived mesenchymal progenitors (hES-MPs) were maintained on PCL polyHIPE microspheres for up to 30 days in either basal (BM), supplemented (SM), or osteogenesis induction media (OIM). hES-MP cells were selected for this study as they resemble adult mesenchymal stromal cells (MSCs) and are capable of long-term proliferation and trilineage differentiation.<sup>20,22,44–47</sup> Over time, cells and

microspheres formed aggregates in all media compositions, although this occurred most rapidly in SM and OIM, the formulations supplemented with an additional 50  $\mu\text{g mL}^{-1}$  of ascorbic acid 2-phosphate (Fig. 2A). Whilst cultures maintained in basal media (BM) eventually also formed aggregates, faster aggregation may have been due to increased collagen production in ascorbic acid replete media due to its role as a cofactor for lysyl hydroxylase and prolyl hydroxylase; enzymes essential for extracellular collagen stabilisation *via* crosslinking.<sup>48</sup> Therefore, to our knowledge, this is the first time degradable polyHIPE microspheres that support mammalian cell culture directly, without modification, have been produced from a clinically relevant biomaterial; a key step towards translation to clinical applications. These PCL microspheres will still need regulatory approval prior to clinical use, but previous clinical translations of PCL-based products facilitate this process<sup>49–51</sup>

To investigate whether cells penetrated the interconnected porous network of the polyHIPE, microsphere aggregates were removed from culture at five-day intervals from day 10 and assessed histologically (Fig. 2B). In BM, there was no significant difference in cell number within the microsphere at day 10 *vs.* day 30, with cells mainly residing in the peripheral pores despite the presence of interconnected porosity. The greatest cellular penetration occurred in SM and OIM, with significantly more cells within the porous network at days 15, 25, and 30 than day 10 in both media ( $p < 0.05$ ). To investigate whether there was any difference in the distance cells penetrated the microsphere, only cells further than 2 or 4 mean pore diameters





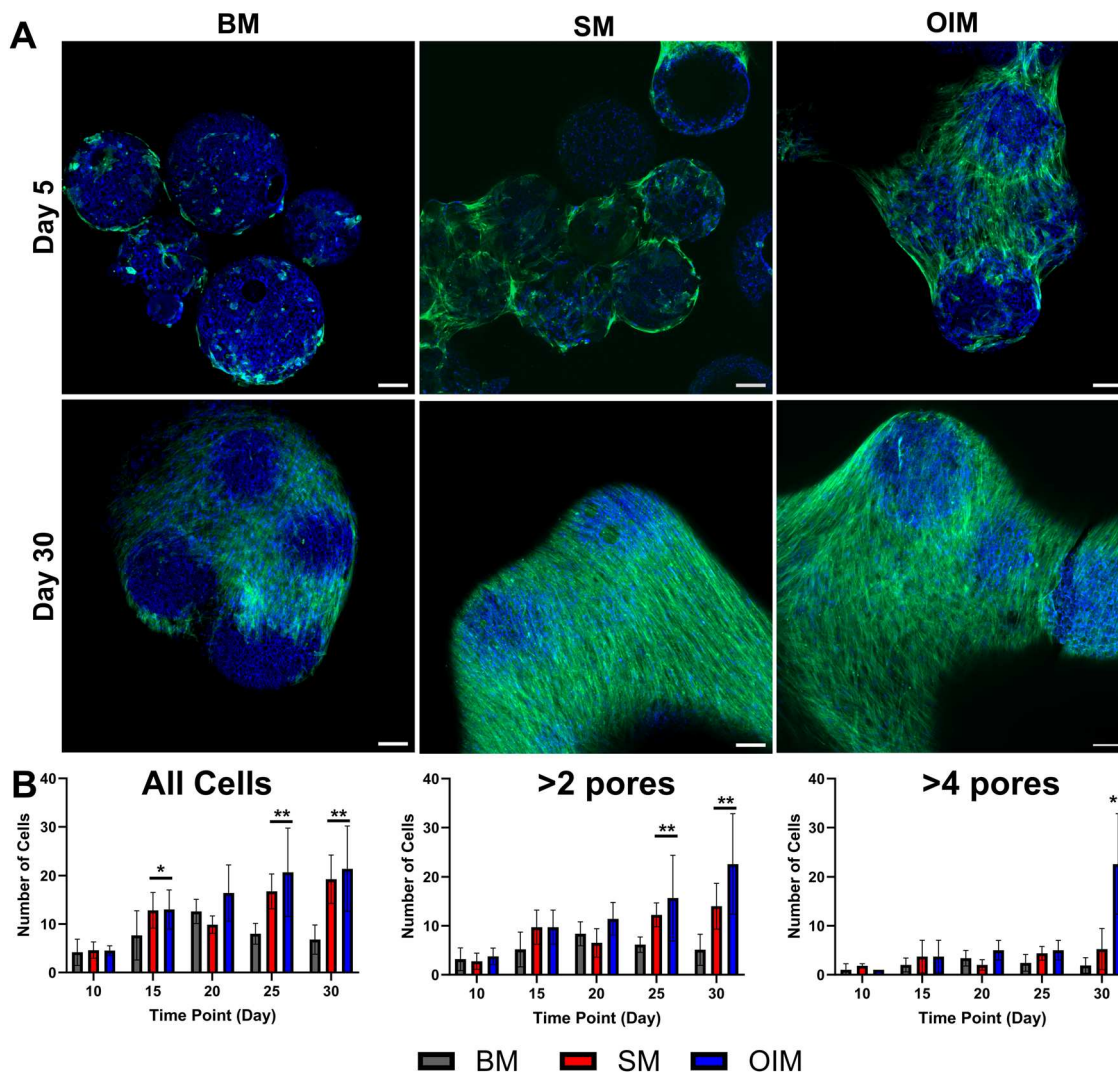


**Fig. 2** Infiltration of hES-MP cells into PCL polyHIPE microspheres. In comparison to BM, cells maintained in SM and OIM formed aggregates by (A) day 5, although all media supported agglomeration by day 30. (green: f-actin (FITC-phalloidin), blue: nuclei/material (DAPI/autofluorescence), scale bars: 200  $\mu\text{m}$ ). (B) Counts of cell penetration into the interconnected network were significantly higher in SM and OIM than BM. When excluding cells at the periphery (2 or 4 mean pore diameters into the particle), the deepest penetrations were observed in OIM.

(47.0/94.0  $\mu\text{m}$ ) into the microsphere were counted. It was observed that cells maintained in dexamethasone-replete media (OIM) demonstrated the deepest penetration, with significantly more cells in the far interior at day 30 than the other media compositions, an observation consistent with previous work on non-biodegradable polyHIPE microspheres<sup>24</sup>

#### PCL polyHIPE microspheres supported mineralised matrix deposition

To assess osteogenesis, histological staining of cells maintained in all three media compositions was performed at day 30 (Fig. 3). In all media, a mass of cells encasing the microspheres and forming the agglomerates was observed. However, a collagenous extracellular matrix (ECM) was only observed in ascorbic acid 2-phosphate-replete media (SM and OIM) (Fig. 3B–D), with the greatest observed in OIM. Positive extracellular calcium staining indicating a mineralising, bone-like ECM only occurred in OIM

(Fig. 3G), with red nodules apparent both at the periphery of the microspheres (Fig. 3H) and in the surrounding cell mass.

Cells infiltrated the furthest into the interconnected micro-porous network of the polyHIPE microspheres when maintained in media containing dexamethasone (OIM), a potent stimulator of osteogenic differentiation through its induction of Runx2 expression.<sup>52</sup> Furthermore, calcium deposition, evidence of osteoblastic differentiation, also only occurred in this media formulation. Therefore, it appears that although cells can deposit a collagenous ECM and infiltrate into the microspheres in non-osteogenic media, commitment to osteoblastic differentiation enhances ECM productions and promotes infiltration.

#### Cells within the microsphere porous network present an osteocyte-like phenotype

During histological evaluation of cellular penetration and extracellular matrix deposition, some cells deep within the



microporous network were observed presenting a “stellate”, osteocyte-like morphology<sup>53</sup> (Fig. 4A–C). *In vivo*, these mature osteoblast-lineage cells act as orchestrators of bone remodelling and mineral homeostasis<sup>54</sup> through an interconnected network of cells, with the cell body residing within lacunae and dendritic processes extending through the canalicular system, connecting osteocytes together. Through SEM imaging, it was observed that cells with this phenotype residing within deep pores connected to their neighbours through processes extending through the smaller interconnecting windows of the micropores (Fig. 4D and E). Here, we observed a mean pore diameter of 23.8  $\mu\text{m}$  and mean interconnect diameter of 6.4  $\mu\text{m}$ , comparable to the reported dimensions of lacunae and canaliculi in human bone ( $\sim 20$   $\mu\text{m}$  and 0.5  $\mu\text{m}$ , respectively).<sup>55</sup> Whilst the polyHIPE interconnects are an order of magnitude larger than native canaliculi, smaller interconnects would not permit cellular infiltration into the interior of the microsphere. The occurrence of this phenotype only within the deeper regions of the microsphere suggests that this microarchitecture that resembles the pore sizes of the lacunar-canalicular system may have presented a 3D environment that facilitated osteocytogenesis.

To further investigate this observation, qPCR was performed at days 15 and 30, revealing significant upregulation of osteoblast-lineage genes when cells were maintained in OIM. Expression of osteocalcin,<sup>56</sup> a mature osteoblast marker, and sclerostin,<sup>57</sup> a late osteocyte marker, both increased 50% between days 15 and 30, with expression of *Dmp-1*, an early osteocyte marker,<sup>58</sup> remaining constant. Sclerostin is a protein produced only by osteocytes that acts to reduce bone formation through negative regulation of Wnt signalling.<sup>59</sup> Here, matrix mineralisation occurred primarily at the periphery of the microspheres and in the matrix, holding microspheres together, although some calcium staining was observed deeper into the microsphere. Production of sclerostin by osteocyte-like cells deep within the particle may partly explain the calcium

distribution, although it could also be due to reduced diffusion of supplements such as  $\beta\text{GP}$  required for mineralisation to the core of the microsphere.

Culture of osteocytes *in vitro* is challenging, with extraction of viable primary osteocytes from their embedded location within hard, mineralised tissues being extremely difficult<sup>60</sup> and limited commercially available cell lines (e.g. IDG-SW3,<sup>58,61</sup> MLO-Y4<sup>62</sup>) available to study this cell type. Differentiation of mesenchymal progenitors and osteoblasts into cells with an osteocyte-like phenotype *in vitro* is also challenging, although extended cultures in osteogenic media have reported comparable cell morphologies and upregulation of osteocyte-related gene expression.<sup>63–66</sup> To observe whether the phenomenon of osteocyte-like cells derived from hES-MPs was specific to the PCL polyHIPE used or would occur on polyHIPE matrices formed from other materials, cultures were repeated for 60 days on our previously reported non-biodegradable polyHIPE microspheres where similar stellate morphologies had been observed.<sup>24</sup> By antibody/3,3'-diaminobenzidine (DAB) staining these sections and quantitatively assessing the intensity of the stain, it was observed that some stellate cells within the microspheres had significantly more sclerostin than others within the microspheres, and that all cells measured within the microsphere were significantly darker than those immediately outside the periphery of the microsphere (Fig. 5).

Sclerostin staining in our positive control (Fig. 5C) is comparable to other antibody/DAB staining of native osteocytes in bone.<sup>67–69</sup> In combination, upregulation of gene-level of expression of osteocyte-related markers in PCL polyHIPE microspheres and positive protein-level staining of sclerostin in stellate morphology cells in non-degradable polyHIPE microsphere indicate that hES-MPs are capable of undergoing osteocytogenesis. However, for this to occur, they seem to require a conducive 3D physical environment, such as that provided by the morphology of these polyHIPE matrices, as well as osteogenic (dexamethasone replete) culture conditions.

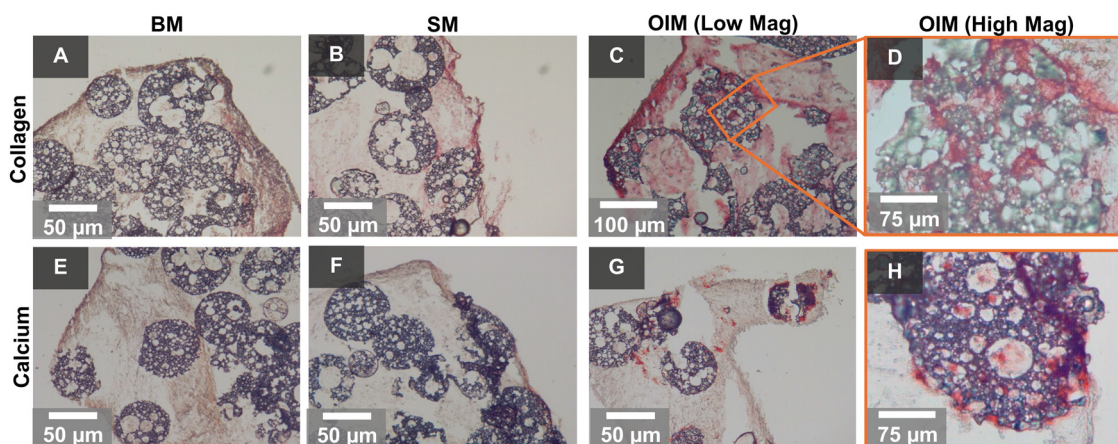


**Fig. 3** Histological evaluation of osteogenesis. Representative collagen staining (Direct Red 80) of hES-MPs cultured on microspheres for 30 days in (A) BM, (B) SM, and (C) and (D) (OIM). Only SM and OIM supported collagenous matrix formation, with the most observed in OIM. Representative calcium staining (Alizarin Red S) of hES-MPs cultured on microspheres for 30 days in (E) BM, (F) SM, and (G) and (H) (OIM). Only OIM supported calcium deposition, indicating formation of a bone-like mineralised extracellular matrix. All sections are 10  $\mu\text{m}$  thick.





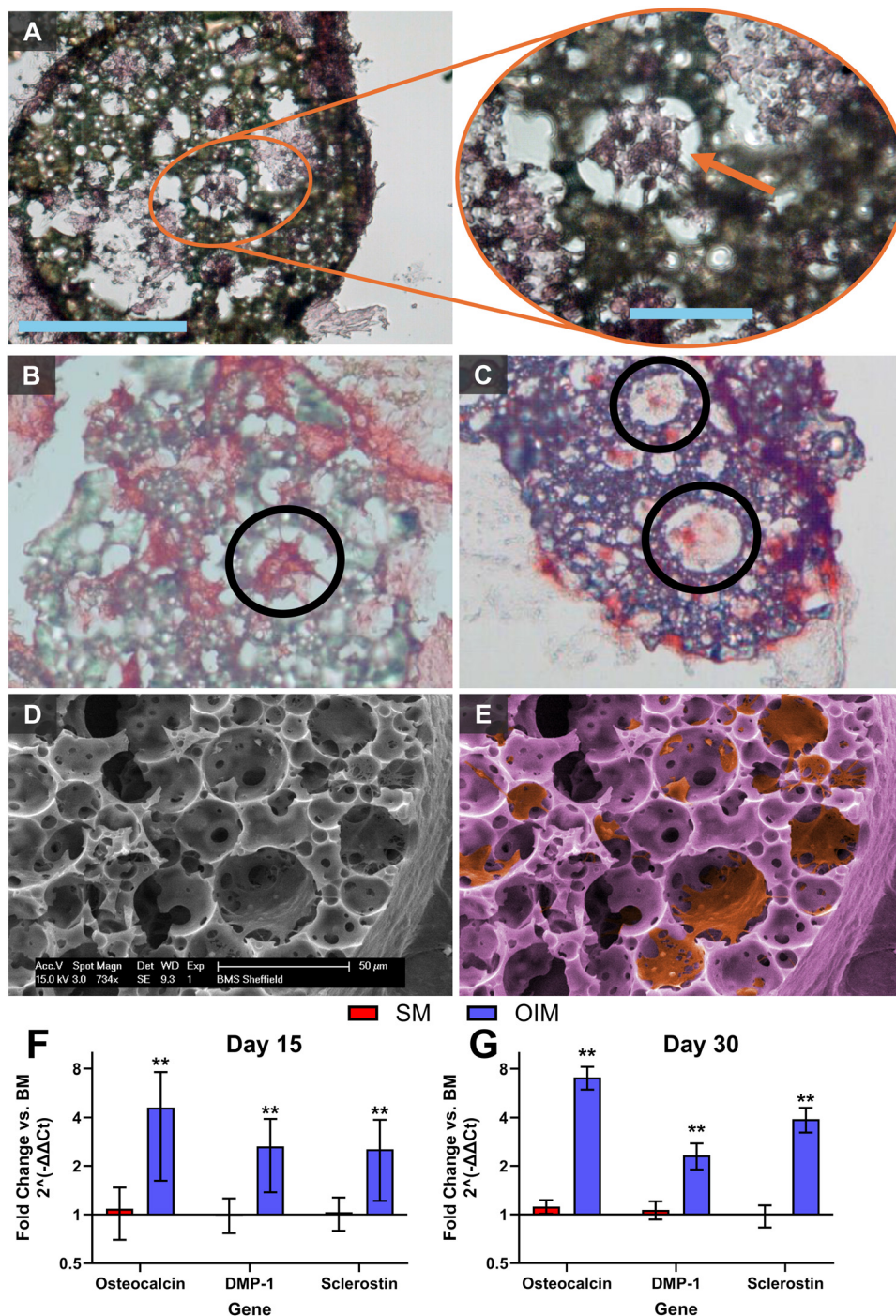


Fig. 4 Osteocyte-like morphologies within polyHIPE microspheres. Stellate morphologies (circled) apparent in histological sections stained with (A) H&E, (B) Direct Red 80, and (C) Alizarin Red S. (D) SEM with (E) false colour to improve contrast reveal osteocyte-like cells connect *via* processes through interconnecting windows between micropores. qPCR at (F) day 15 and (G) 30 reveal significant expression of late osteoblast-lineage genes when maintained in OIM, including sclerostin, a late osteocyte marker.

### PolyHIPE microspheres improve injected cell survival and support angiogenesis

Whilst porous polymer microspheres hold promise as an acellular bone graft substitute material, they also hold potential as a carrier for injectable cell therapies for skeletal repair. To assess the amenability of this PCL polyHIPE microsphere

system to this application, cell survival post injection with polyHIPE microspheres was compared to their non-porous counterparts and ‘unconfined’ cells in suspension. Cells were either injected ‘unconfined’ or cultured on microspheres for 4 days prior to injection through a 21G needle. Immediately post-injection, cells were dissociated, and viable cell counts made.



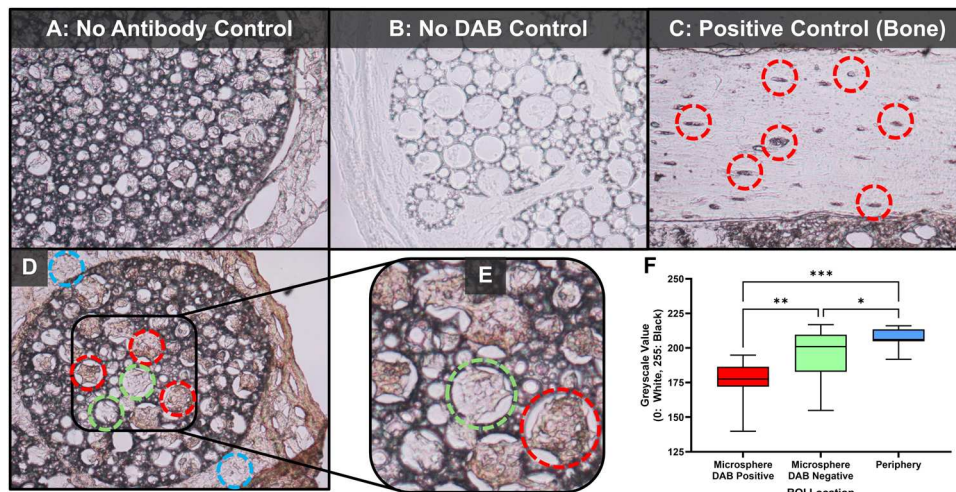


**Fig. 5** Osteocyte-like cells within non-degradable polyHIPE microspheres produce significantly more sclerostin than those immediately outside the microspheres. (A) No observable difference in cell staining in the control without antibody or (B) DAB control. (C) Staining of native murine cortical bone reveals positive sclerostin staining in the bone lacunae. (D) Low and (E) high magnification representative image of an antibody/DAB staining microsphere section. Red: positive cell, green: negative cell, blue: cells immediately outside microsphere periphery. (F) Converting images to greyscale and measuring a central ROI in positive, negative and external cells revealed a sub-population of internal cells displayed significantly higher sclerostin abundance than their neighbours, and all internal cells had significantly higher sclerostin than those immediately outside the microsphere ( $N = 4$ ,  $n = 15$ ).

Only porous, polyHIPE PCL microspheres were able to provide a protective environment, with no significant difference to the ‘unconfined’ cell control. In contrast, significantly reduced cell survival of only 79.6% was observed on solid PCL microspheres (Fig. 6A). The ability to for cells to grow into the porous microsphere interior may explain why only this variant of PCL microspheres protected cells during injection, with cells residing within the particle being further from the fluid shear stress exerted during injection,<sup>70</sup> indicating the suitability of these microspheres as a carrier for injectable cell therapies.

To assess vascularisation, an ‘unconfined’ hES-MP suspension, and non-porous and polyHIPE PCL microspheres pre-cultured using the same method, were injected into the chorioallantoic membrane (CAM) of a fertilised chicken egg. The use of the CAM assay is a relatively simple way to assess the angiogenic potential of new biomaterials as it is legally not considered an animal model, yet still provides an *in vivo* environment with complex vasculature.<sup>71,72</sup> After 7 days, both microsphere types supported greater neo-vasculature formation than ‘unconfined’ cells (Fig. 6B), with no significant difference between the porous and non-porous versions despite the difference in microarchitecture (Fig. 6C). As our PCL-M release no factors known to directly stimulate angiogenesis (*e.g.* vascular endothelial growth factor) and we observed no significant difference in porous and non-porous microspheres, we hypothesise that cell-laden microspheres caused an increase in blood vessel infiltration *versus* ‘unconfined’ cells due to the retention of cells within a specific location in the CAM causing an oxygen gradient. This localised hypoxia may have stimulated the release of hypoxia-inducible factors (HIFs) which are known to drive angiogenesis.<sup>73</sup> New blood vessel infiltration into the microsphere agglomerates was apparent from macroscopic brightfield images (Fig. 6E and F), but histological analysis of

explanted particles revealed continuous tissue growth across the implant site, whereas solid polymer microspheres had voids similar to other comparable microsphere architectures.<sup>4,15</sup>

## Conclusions

In summary, highly porous, biodegradable microspheres were successfully generated that supported mesenchymal progenitor cell culture over extended time periods (30 days). When maintained in osteogenesis induction media, cells underwent differentiation and penetrated deep within the interconnected microporous architecture. Bone-like mineralised extracellular matrix was deposited both within the microspheres and between them, forming cell-microsphere agglomerates. It was observed some differentiated cells within the microspheres had a “stellate”, osteocyte-like morphology along with mRNA expression and protein synthesis of osteocyte specific markers, suggesting the polyHIPE microsphere architecture facilitated the differentiation of mature bone cell phenotypes. Finally, when microspheres were injected with cells, porous microspheres significantly improved cell survival in comparison to non-porous controls, and stimulated angiogenesis in a CAM model. To conclude, these biodegradable, porous polymer microspheres support mature bone-like tissue formation and present a promising opportunity to expand our range of synthetic bone graft substitutes.

## Experimental

### Materials

Polycaprolactone (PCL) triol ( $M_n \sim 900$ ), trimethylamine (TEA), methacrylic anhydride, diphenyl(2,4,6-trimethylbenzoyl)phosphine oxide/2-hydroxy-2-methylpropiophenone, (50:50), 2-ethylhexyl





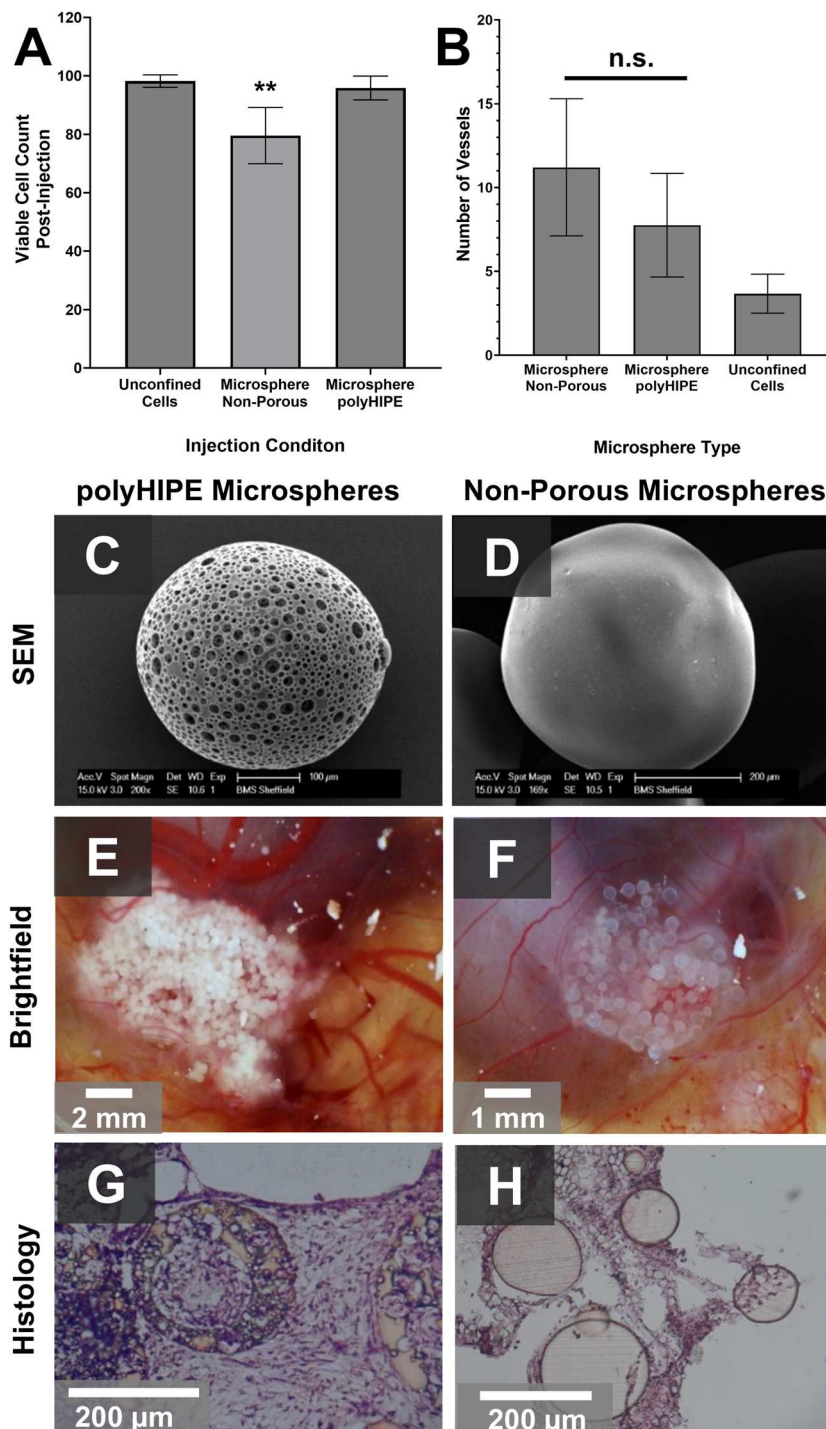


**Fig. 6** Injected cell survival and angiogenesis. (A) Cell viability comparable to injection of 'unconfined' cells was only achieved through polyHIPE microspheres, with a significantly reduced cell survival on non-porous microspheres. (B) When implanted into a chick chorioallantoic membrane for 7 days, greater blood vessel infiltration was observed in the presence of microspheres, with no significant difference between polyHIPE and non-porous structures. SEM images demonstrate the difference in microarchitecture between (C) polyHIPE and (D) non-porous microspheres. Macroscopic images show blood vessel formation into both (E) polyHIPE and (F) non-porous microspheres, but histology (H&E) reveals that continuous tissue formation is only achieved in (G) polyHIPE particles, with cells surrounding but not penetrating (H) non-porous variants.

acrylate (EHA), isobornyl acrylate (IBOA), trimethylolpropane triacrylate (TMPTA), sodium hydroxide (NaOH), penicillin-streptomycin, L-glutamine, dexamethasone  $\beta$ -glycerophosphate, ascorbic acid(2-phosphate), phosphate buffered saline (PBS), formaldehyde,

Triton X-100, haematoxylin and eosin (H&E), Alizarin Red S, Direct Red 80, hexamethyldisilane (HMDS), bovine serum albumin (BSA), and trypan blue were purchased from Sigma-Aldrich/Merck, UK.



Dichloromethane (DCM), methanol, chloroform, toluene, ethanol, xylene, FITC-phalloidin, and 4',6-diamidino-2-phenylindole (DAPI) were purchased from Fischer Scientific, UK. Hypermer B246 was kindly donated by Croda, UK.

Human embryonic stem-cell derived mesenchymal progenitor cells (hES-MPs) were sourced from Cellartis, Sweden. Alpha modification of Eagle's medium ( $\alpha$ -MEM) was purchased from Lonza, UK, foetal bovine serum (FBS) from Labtech, UK, and human basic fibroblast growth factor (hFGF) from (Life Technologies, UK). Tissue freezing medium was acquired from Leica. RNAqueous 4PCR Kits were purchased from Ambion, UK, first strand cDNA synthesis kit from (GE Healthcare, UK), and SYBR green PCR master mix and primers from Eurogentec, UK. Rabbit anti-sclerostin antibody (ab85799) and a mouse and rabbit specific HRP/DAB detection IHC kit (ab64264) were purchased from Abcam, UK. Fertilised chicken eggs were purchased from Medeggs, UK, and maintained in a humidified egg incubator (R-COM Suro20).

## Methods

**Polycaprolactone methacrylation.** Commercially available PCL was methacrylated *via* a modification of the process described previously.<sup>26</sup> Briefly, PCL triol (30.0 g) was dissolved in a solution of DCM and TEA (120 mL and 17.4 g (6 molar equivalent), respectively) and cooled in an ice bath. Methacrylic anhydride (28.2 g, 6 molar equivalent) dissolved in 50 mL DCM was added dropwise, then the reaction brought to room temperature and left to react for 24 h under constant stirring. Residual DCM and TEA were removed by rotary evaporation before dissolving the residual pre-polymer dissolved in excess methanol. The solution was purified by three precipitations at  $-80$  °C, removing the methanol-containing contaminants after each freeze and redissolving the PCL methacrylate (PCL-M) in fresh methanol. The final PCL-M was rotary evaporated to constant mass to remove residual methanol. This reaction duration and molar ratio yields a PCL-M with an  $\sim 47\%$  degree of methacrylation.<sup>36</sup>

**PCL HIPE formulation.** To form the photocurable continuous phase, 3 g of PCL-M and 0.3 g of surfactant (Hypermer B246) were combined in a vessel at 40 °C until the surfactant had dissolved. Once cooled to room temperature, 0.15 g photoinitiator (diphenyl(2,4,6-trimethylbenzoyl)phosphine oxide/2-hydroxy-2-methylpropiophenone, 50:50), 3 g chloroform and 0.5 g toluene were added. To form the HIPE, 1 mL was transferred to a new vial and stirred at 350 rpm at 35 °C with dropwise addition of 4 mL of deionised water ( $\text{dH}_2\text{O}$ ) over a 5-minute period.

**PolyHIPE microsphere manufacture.** Manufacturing of PCL microspheres was based on previously established parameters.<sup>24</sup> 2 mL of HIPE solution was shear separated to form droplets through dropwise addition to a stirred beaker (320 rpm) of  $\text{dH}_2\text{O}$  using a micropipette, forming a double emulsion (w/o/w). Once fully added, the double emulsion was stirred for a further 2 minutes before immediate photopolymerisation for 60 seconds (Omnicure S1000, 100 W), converting the HIPE droplets to polyHIPE microspheres. Solid microspheres were produced as above, but from the photocurable continuous phase only. Microspheres were removed

by filtration, washed in water 3 times for 15 minutes each then sieved to retain only microspheres below 500  $\mu\text{m}$  diameter.

**Microsphere physical characterisation.** To quantify diameter, microspheres were imaged under an inverted light microscope and a scale set using a micrometer. 50 microspheres per image across ten images were measured using ImageJ ( $n = 500$ ).<sup>74</sup> Circularity was assessed by segmenting microspheres as primary objects using CellProfiler and measuring their eccentricity ( $n = 161$ ).<sup>75</sup>

Pore and interconnect diameters were calculated using Pore D<sup>2</sup>, a deep learning tool for assessment of polyHIPEs.<sup>34</sup> 10 SEM images of microsphere cross sections were quantified, measuring 1244 pores and 1294 interconnects. Pore diameters were multiplied by a statistical correction factor to represent the equatorial void diameter as it is not known how close to the equator the pore has been bisected.<sup>20</sup>

**PCL degradation.** Standard ( $\text{dH}_2\text{O}$ ) and accelerated (0.1 M NaOH) degradation media were used to assess degradability of PCL polyHIPE microspheres. 0.2 g of microspheres were added to each media or stored dry as a control, then maintained at 37 °C for 60 days. Solutions were removed, particles dried to constant mass, and then a final weight taken to determine material loss.

**Cell culture.** Human embryonic stem-cell derived mesenchymal progenitor (hES-MP) cells were used for all experiments and maintained under standard conditions (37 °C, 5%  $\text{CO}_2$  humidified incubator, culture medium changed every 2–3 days). Cells were maintained in basal media (BM), formulated from alpha modification of Eagle's medium ( $\alpha$ -MEM) supplemented with 10% foetal bovine serum (FBS), 100  $\text{mg mL}^{-1}$  penicillin–streptomycin, 2 mM L-glutamine, and 4  $\text{ng mL}^{-1}$  human basic fibroblast growth factor (hFGF). For osteogenesis studies, cells were also maintained in either osteogenesis induction media (OIM, BM supplemented with 100 nM dexamethasone, 5 mM  $\beta$ -glycerophosphate, and 50  $\mu\text{g mL}^{-1}$  ascorbic acid 2-phosphate), or supplemented media (SM), which is OIM without dexamethasone.

For cell culture, microspheres were sterilised in 70% ethanol for 1 hour, rinsed three times in PBS, and soaked in BM for one hour before seeding. To seed, 100 000 cells were added to 0.2 g of microspheres in a T25 and gently rocked for 45 minutes at 12 oscillations per minute in an incubator. They were then maintained under static conditions for a further 2 hours before gently rinsing with PBS and transfer to BM in a new T25. 80% of media was replaced every 2–3 days to prevent loss of microspheres.

**Confocal microscopy.** To image cell-microsphere agglomerates, samples were taken on days 5 and 30, rinsed three times PBS, fixed in 3.7% formaldehyde for 1 hour, permeabilised for 15 minutes (0.1% Triton X-100 in PBS), then washed three times in PBS. Cytoskeleton (f-actin) and nuclei were stained with FITC-phalloidin and DAPI, respectively, for 1 hour before rinsing with PBS three times. Samples were mounted on coverslips, then imaged using a Zeiss LSM 510META upright confocal microscope, capturing 1024  $\times$  1024 pixel images with a 10 $\times$  objective (Achromplan 10 $\times$ /0.3 W, Carl Zeiss Ltd, UK) at Ex: 488 nm/Em: 505 nm (phalloidin) and Ex: 760 nm, Em: 435–485 nm (nuclei).



**Quantifying cellular penetration.** For quantification, samples were taken every 5 days from days 5–30, rinsed three times PBS, fixed in 3.7% formaldehyde for 1 hour, then washed three further times in PBS. For histology, samples were submerged in tissue freezing medium and frozen by dipping in liquid nitrogen. Samples were then stored in a  $-80\text{ }^{\circ}\text{C}$  freezer for a minimum of 24 hours before sectioning using a cryostat (Leica CM1860 UV) at  $-24\text{ }^{\circ}\text{C}$  and  $10\text{ }\mu\text{m}$  thickness. Samples were stained with haematoxylin and eosin (H&E), Alizarin Red S (calcium) or Direct Red 80 (collagen) and imaged under an optical microscope (B5 professional series, Motic). Number and distance of all cells penetrating into each microsphere in each section was measured using ImageJ.<sup>74</sup>

**Scanning electron microscopy.** SEM was used to assess cell morphology inside microspheres. Cell-containing samples were sectioned as above, then mounted on 12 mm glass coverslips, and dehydrated through a series of solutions of increasing ethanol content in  $\text{dH}_2\text{O}$  (35%, 60%, 80%, 90% and 100%, 15 min per solution). Finally, samples were exposed to HMDS in ethanol (50 : 50) for 1 hour, then 100% HMDS for five minutes twice, before air drying for 1 hour. Samples were then gold coated and imaged with an SEM (Philips/FEI XL30 ESEM).

**Osteoblast-lineage gene expression.** Assessment of osteoblast and osteocyte genes was performed on days 15 and 30 as previously described.<sup>76</sup> Briefly, RNA was extracted using RNAqueous 4PCR Kits according to manufacturer's instructions.  $2\text{ }\mu\text{g}$  of RNA was used for reverse transcription using the first strand cDNA synthesis kit and quantitative real-time polymerase chain reactions (RT-PCR) performed using SYBR green PCR master mix and  $0.1\text{ }\mu\text{M}$  primers (L32) (housekeeping, F: 5'-GGGAGAGACCCG TCTGAACA-3' R: 5'-GAACCACGATGGTCGCTTTC-3'), osteocalcin (F: 5'-CAATCCGGACTGTGACGAGTT-3', R: 5'-CCTAGACCCGGCC GTAGAAG-3'), Dmp-1 (F: 5'-GAGCAGTGAGTCATCAGAAAGC-3', R: 5'-GAGAAGCCACCAGCTAGCCTAT-3'), sclerostin (SOST, F: 5'-CCG GAGCTGGAGAACAACAAG-3', R: 5'-GCAGTGGCCGGAGCACACC-3'). PCR amplification was carried out according to the following conditions:  $50\text{ }^{\circ}\text{C}$  for 2 minutes,  $95\text{ }^{\circ}\text{C}$  for 10 minutes (1 cycle);  $95\text{ }^{\circ}\text{C}$  for 15 seconds,  $60\text{ }^{\circ}\text{C}$  for 1 minute, (40 cycles). Data were analysed using SDS 2.0 software.

**Non-degradable HIPE formulation.** To assess whether cell response was due to the chemistry or morphology of the PCL polyHIPE, non-degradable polyHIPE particles were formed from an EHA and IBOA-based HIPE, as previously described.<sup>20,24</sup> Briefly, to form the continuous phase, a monomer mixture (30 wt% EHA, 70 wt% IBOA) was blended, then the crosslinker trimethylolpropane triacrylate TMPTA added at 27 wt%. A surfactant (Hypermer B246) and photoinitiator (diphenyl(2,4,6-trimethylbenzoyl)phosphine oxide/2-hydroxy-2-methylpropiophenone, 50 : 50) were dissolved at 3 wt% and 5 wt% of the monomers and crosslinker, respectively. To prepare the HIPE for microsphere manufacture, 1 mL was transferred to a new vial and stirred at 350 rpm at  $35\text{ }^{\circ}\text{C}$  with dropwise addition of 4 mL of deionised water ( $\text{dH}_2\text{O}$ ) over a 5-minute period.

**3,3'-Diaminobenzidine staining of sclerostin.** Sclerostin staining was performed at day 60 on non-degradable polyHIPE microsphere cultures maintained in OIM using a rabbit anti-sclerostin antibody (ab85799, Abcam, UK) and a mouse and

rabbit specific HRP/DAB detection IHC kit (ab64264, Abcam, UK). Sections of a native Wistar rat tibia embedded in paraffin collected from a previous study were used as a positive control. Sectioned samples of microspheres were protein blocked for 10 minutes, washed, submerged in a hydrogen peroxide block for 5 minutes to inhibit endogenous peroxidases, then washed again. The primary rabbit anti-sclerostin antibody was diluted in buffer (PBS, 1% bovine serum albumin) at 1 : 350 and added to the samples for 12 hours at  $4\text{ }^{\circ}\text{C}$ . Samples were washed 5 times with PBS for 5 minutes each wash, then a biotinylated goat anti-rabbit antibody (1 : 300 in buffer) was added for 1 hour before removal and washing 3 times in PBS for 5 minutes each wash. The 3,3'-diaminobenzidine (DAB) stain was then added for 5 minutes precisely before washing 3 times in PBS for 5 minutes each wash. Tibiae sections were dewaxed in xylene before undergoing the same process as above. No antibody and DAB-only controls were also performed to ensure specificity. Brightfield images were captured under an optical microscope (B5 professional series, Motic) with constant exposure time.

For quantification, brightfield images were converted to 8-bit greyscale using ImageJ. Cells within the microsphere in the sections that were visibly darker were qualitatively assigned as 'DAB positive', with the remainder assigned 'DAB negative'. A 50-pixel diameter region of interest (ROI) was placed centrally on 15 DAB positive cells, 15 DAB negative cells, and 15 regions immediately outside the periphery of the microsphere, measuring the mean greyscale value in each ROI.

**Injected cell survival.** Cells were seeded on porous or solid microspheres as above and maintained in BM for 4 days. Half of the particles had cells dissociated with trypsin and viable cell counts taken by Trypan Blue staining and counting with a haemocytometer, with the other half drawn into a 20 mL syringe and passed through a 21G needle before dissociation and counting. The number of live cells obtained from the injected microspheres was normalised against the non-injected, with 20 000 'unconfined' hES-MP cells treated the same as the microsphere-sourced cells used as a control.

**Vascularisation.** The chorioallantoic membrane (CAM) assay was performed with fertilised chicken eggs (*Gallus domesticus*) incubated from day 2 of fertilisation until day 8 at  $37\text{ }^{\circ}\text{C}$  in a humidified egg incubator.<sup>77</sup> At day 8, a window was cut into the shell of the egg ( $5\text{ mm}^2$ ) and 100 000 'unconfined' cells or 0.5 g precultured microspheres (3 days in OIM) in PBS were injected into the opening using a 5 mL syringe with a 17G needle. Masking tape was used to secure sterilised (in ethanol, 30 minutes) parafilm over the implantation site to prevent infections.

**Statistics.** All statistical analyses and data visualisations were produced in Graphpad Prism (v10.2.3). Depending on the number of independent variables, significant differences were evaluated with either one- or two-way ANOVA with Holm-Šidák's post-test for multiple comparisons. qPCR comparisons are made from  $\Delta\Delta\text{CT}$  values to retain normally distributed values for analysis. All data are presented as mean  $\pm$  SD.  $p < 0.05$  (\*) was considered significant, and  $p$  values  $< 0.01$  are noted as \*\*. All experiments were repeated a minimum of twice in triplicate ( $N = 2, n = 3$ ).





## Author contributions

TEP: conceptualization; methodology, investigation, writing – original draft, visualization. RO: formal analysis, writing – original draft, writing – review & editing, visualization, funding acquisition. CS: investigation, methodology, supervision. HB: investigation. ALH: investigation. NG: methodology. GR: methodology, resources, writing – review & editing, supervision. FC: conceptualization, methodology, resources, writing – review & editing, supervision, project administration, funding acquisition.

## Data availability

The data supporting this article have been included in the ESI.†

## Conflicts of interest

The authors have no conflicts of interest to declare.

## Acknowledgements

We acknowledge funding from the Engineering and Physical Sciences Research Council (EPSRC) for studentships for TEP and CS via a Doctoral Training Account. ALH was supported by the University of Sheffield. FC thanks the Royal Society for funding of a Sheffield Faculty Studentship and a Royal Society Leverhulme Trust Senior Research Fellowship 2022 (SRF\R1\221053). RO would like to thank the University of Nottingham for the award of a Nottingham Research Fellowship. Confocal imaging was performed at the Kroto Imaging Facility.

## References

- 1 S. Kanwar and S. Vijayavenkataraman, Design of 3D printed scaffolds for bone tissue engineering: a review, *Bioprinting*, 2021, **24**, e00167.
- 2 C. E. Gillman and A. C. Jayasuriya, FDA-approved bone grafts and bone graft substitute devices in bone regeneration, *Mater. Sci. Eng., C*, 2021, **130**, 112466.
- 3 T. Kurien, R. G. Pearson and B. E. Scammell, Bone graft substitutes currently available in orthopaedic practice, *Bone Joint J.*, 2013, **95-B**(5), 583–597.
- 4 H.-S. Sohn and J.-K. Oh, Review of bone graft and bone substitutes with an emphasis on fracture surgeries, *Biomater. Res.*, 2019, **23**(1), 9.
- 5 M. Alonzo, *et al.*, Bone tissue engineering techniques, advances, and scaffolds for treatment of bone defects, *Curr. Opin. Biomed. Eng.*, 2021, **17**, 100248.
- 6 S. Bhushan, *et al.*, Scaffold Fabrication Techniques of Biomaterials for Bone Tissue Engineering: A Critical Review, *Bioengineering*, 2022, **9**, 728.
- 7 G. L. Koons, M. Diba and A. G. Mikos, Materials design for bone-tissue engineering, *Nat. Rev. Mater.*, 2020, **5**(8), 584–603.
- 8 Z. Cai, *et al.*, Microspheres in bone regeneration: Fabrication, properties and applications, *Mater. Today Adv.*, 2022, **16**, 100315.
- 9 H. Wang, *et al.*, The use of micro- and nanospheres as functional components for bone tissue regeneration, *Tissue Eng., Part B*, 2012, **18**(1), 24–39.
- 10 J. E. Barthold, *et al.*, Recellularization and Integration of Dense Extracellular Matrix by Percolation of Tissue Micro-particles, *Adv. Funct. Mater.*, 2021, **31**(35), 2103355.
- 11 A. A. Sherstneva, *et al.*, Biodegradable Microparticles for Regenerative Medicine: A State of the Art and Trends to Clinical Application, *Polymers*, 2022, **14**(7), 1314.
- 12 M. B. Oliveira and J. F. Mano, Polymer-based microparticles in tissue engineering and regenerative medicine, *Biotechnol. Prog.*, 2011, **27**(4), 897–912.
- 13 Z. Zhou, *et al.*, Polymer-based porous microcarriers as cell delivery systems for applications in bone and cartilage tissue engineering, *Int. Mater. Rev.*, 2021, **66**(2), 77–113.
- 14 T. Jiang, *et al.*, Chitosan-poly(lactide-co-glycolide) microsphere-based scaffolds for bone tissue engineering: In vitro degradation and in vivo bone regeneration studies, *Acta Biomater.*, 2010, **6**(9), 3457–3470.
- 15 M. H. Amer, *et al.*, Designing topographically textured microparticles for induction and modulation of osteogenesis in mesenchymal stem cell engineering, *Biomaterials*, 2021, **266**, 120450.
- 16 J. M. Melero-Martin, *et al.*, Expansion of chondroprogenitor cells on macroporous microcarriers as an alternative to conventional monolayer systems, *Biomaterials*, 2006, **27**(15), 2970–2979.
- 17 R. K. Kankala, *et al.*, Highly Porous Microcarriers for Minimally Invasive In Situ Skeletal Muscle Cell Delivery, *Small*, 2019, **15**(25), 1901397.
- 18 B. Aldemir Dikici and F. Claeysens, Basic Principles of Emulsion Templating and Its Use as an Emerging Manufacturing Method of Tissue Engineering Scaffolds, *Front. Bioeng. Biotechnol.*, 2020, **8**, 875.
- 19 M. S. Silverstein, PolyHIPES: recent advances in emulsion-templated porous polymers, *Prog. Polym. Sci.*, 2014, **39**(1), 199–234.
- 20 R. Owen, *et al.*, Emulsion templated scaffolds with tunable mechanical properties for bone tissue engineering, *J. Mech. Behav. Biomed. Mater.*, 2016, **54**, 159–172.
- 21 C. Sherborne, *et al.*, Light-based additive manufacturing of PolyHIPES: Controlling the surface porosity for 3D cell culture applications, *Mater. Des.*, 2018, **156**, 494–503.
- 22 H. Bahmaee, *et al.*, Design and Evaluation of an Osteogenesis-on-a-Chip Microfluidic Device Incorporating 3D Cell Culture, *Front. Bioeng. Biotechnol.*, 2020, **8**, 557111.
- 23 R. Owen, *et al.*, Combined Porogen Leaching and Emulsion Templating to produce Bone Tissue Engineering Scaffolds, *Int. J. Bioprint.*, 2020, **6**(2), 265.
- 24 T. E. Paterson, *et al.*, Porous microspheres support mesenchymal progenitor cell ingrowth and stimulate angiogenesis, *APL Bioeng.*, 2018, **2**(2), 026103.
- 25 R. Moglia, *et al.*, Solvent-Free Fabrication of polyHIPE Microspheres for Controlled Release of Growth Factors, *Macromol. Rapid Commun.*, 2014, **35**(14), 1301–1305.
- 26 B. Aldemir Dikici, *et al.*, Emulsion templated scaffolds manufactured from photocurable polycaprolactone, *Polymer*, 2019, **175**, 243–254.



- 27 B. Aldemir Dikici, *et al.*, Thiolene- and Polycaprolactone Methacrylate-Based Polymerized High Internal Phase Emulsion (PolyHIPE) Scaffolds for Tissue Engineering, *Biomacromolecules*, 2022, **23**(3), 720–730.
- 28 B. Aldemir Dikici, *et al.*, A Novel Bilayer Polycaprolactone Membrane for Guided Bone Regeneration: Combining Electrospinning and Emulsion Templating, *Materials*, 2019, **12**(16), 2643.
- 29 B. Aldemir Dikici, *et al.*, In Vivo Bone Regeneration Capacity of Multiscale Porous Polycaprolactone-Based High Internal Phase Emulsion (PolyHIPE) Scaffolds in a Rat Calvarial Defect Model, *ACS Appl. Mater. Interfaces*, 2023, **15**(23), 27696–27705.
- 30 M. Whitely, *et al.*, Porous PolyHIPE microspheres for protein delivery from an injectable bone graft, *Acta Biomater.*, 2019, **93**, 169–179.
- 31 Q. Zhang, *et al.*, Preparation of open porous polycaprolactone microspheres and their applications as effective cell carriers in hydrogel system, *Mater. Sci. Eng., C*, 2012, **32**(8), 2589–2595.
- 32 S. Y. Kim, J.-Y. Hwang and U. S. Shin, Preparation of nano/macroporous polycaprolactone microspheres for an injectable cell delivery system using room temperature ionic liquid and camphene, *J. Colloid Interface Sci.*, 2016, **465**, 18–25.
- 33 R. Owen, *et al.*, Computer Vision for Substrate Detection in High-Throughput Biomaterial Screens Using Bright-Field Microscopy, *Adv. Intelligent Syst.*, 2024, **n/a**(n/a), 2400573.
- 34 I. Karaca and B. Aldemir Dikici, Quantitative Evaluation of the Pore and Window Sizes of Tissue Engineering Scaffolds on Scanning Electron Microscope Images Using Deep Learning, *ACS Omega*, 2024, **9**(23), 24695–24706.
- 35 M. Bartnikowski, *et al.*, Degradation mechanisms of polycaprolactone in the context of chemistry, geometry and environment, *Prog. Polym. Sci.*, 2019, **96**, 1–20.
- 36 J. Field, *et al.*, A Tuneable, Photocurable, Poly(Caprolactone)-Based Resin for Tissue Engineering—Synthesis, Characterisation and Use in Stereolithography, *Molecules*, 2021, **26**(5), 1199.
- 37 O. Ozkendir, *et al.*, Engineering periodontal tissue interfaces using multiphasic scaffolds and membranes for guided bone and tissue regeneration, *Biomater. Adv.*, 2024, **157**, 213732.
- 38 V. Gupta, *et al.*, Microsphere-Based Scaffolds in Regenerative Engineering, *Ann. Rev. Biomed. Eng.*, 2017, **19**, 135–161.
- 39 A. Khademhosseini and R. Langer, Microengineered hydrogels for tissue engineering, *Biomaterials*, 2007, **28**(34), 5087–5092.
- 40 A. A. Dundas, *et al.*, Achieving Microparticles with Cell-Instructive Surface Chemistry by Using Tunable Co-Polymer Surfactants, *Adv. Funct. Mater.*, 2020, **30**(36), 2001821.
- 41 W. Li, *et al.*, Microfluidic fabrication of microparticles for biomedical applications, *Chem. Soc. Rev.*, 2018, **47**(15), 5646–5683.
- 42 J. Ferrer, *et al.*, An approach for the scalable production of macroporous polymer beads, *J. Colloid Interface Sci.*, 2022, **616**, 834–845.
- 43 N. J. A. Sloane, The Packing of Spheres, *Sci. Am.*, 1984, **250**(1), 116–125.
- 44 C. Karlsson, *et al.*, Human embryonic stem cell-derived mesenchymal progenitors—potential in regenerative medicine, *Stem Cell Res.*, 2009, **3**(1), 39–50.
- 45 G. M. de Peppo, *et al.*, Human Embryonic Stem Cell-Derived Mesodermal Progenitors Display Substantially Increased Tissue Formation Compared to Human Mesenchymal Stem Cells Under Dynamic Culture Conditions in a Packed Bed/Column Bioreactor, *Tissue Eng., Part A*, 2012, **19**(1–2), 175–187.
- 46 B. Bhaskar, *et al.*, Design and Assessment of a Dynamic Perfusion Bioreactor for Large Bone Tissue Engineering Scaffolds, *Appl. Biochem. Biotechnol.*, 2018, **185**(2), 555–563.
- 47 R. Owen, *et al.*, Comparison of the Anabolic Effects of Reported Osteogenic Compounds on Human Mesenchymal Progenitor-Derived Osteoblasts, *Bioengineering*, 2020, **7**(1), 12.
- 48 S. R. Pinnell, Regulation of collagen biosynthesis by ascorbic acid: a review, *Yale J. Biol. Med.*, 1985, **58**(6), 553–559.
- 49 R. Dwivedi, *et al.*, Polycaprolactone as biomaterial for bone scaffolds: Review of literature, *J. Oral. Biol. Craniofac. Res.*, 2020, **10**(1), 381–388.
- 50 M. O. Christen and F. Vercesi, Polycaprolactone: How a Well-Known and Futuristic Polymer Has Become an Innovative Collagen-Stimulator in Esthetics, *Clin., Cosmet. Invest. Dermatol.*, 2020, **13**, 31–48.
- 51 M. Gharibshahian, *et al.*, Recent advances on 3D-printed PCL-based composite scaffolds for bone tissue engineering, *Front. Bioeng. Biotechnol.*, 2023, **11**, 1168504.
- 52 F. Langenbach and J. Handschel, Effects of dexamethasone, ascorbic acid and  $\beta$ -glycerophosphate on the osteogenic differentiation of stem cells in vitro, *Stem Cell Res. Ther.*, 2013, **4**(5), 117.
- 53 H. Chen, T. Senda and K. Y. Kubo, The osteocyte plays multiple roles in bone remodeling and mineral homeostasis, *Med. Mol. Morphol.*, 2015, **48**(2), 61–68.
- 54 R. Owen and G. C. Reilly, In vitro Models of Bone Remodeling and Associated Disorders, *Front. Bioeng. Biotechnol.*, 2018, **6**, 134.
- 55 B. Yu, *et al.*, Assessment of the human bone lacuno-canalicular network at the nanoscale and impact of spatial resolution, *Sci. Rep.*, 2020, **10**(1), 4567.
- 56 M. L. Zoch, T. L. Clemens and R. C. Riddle, New insights into the biology of osteocalcin, *Bone*, 2016, **82**, 42–49.
- 57 R. L. van Bezooijen, *et al.*, Sclerostin is an osteocyte-expressed negative regulator of bone formation, but not a classical BMP antagonist, *J. Exp. Med.*, 2004, **199**(6), 805–814.
- 58 S. M. Woo, *et al.*, Cell line IDG-SW3 replicates osteoblast-to-late-osteocyte differentiation in vitro and accelerates bone formation in vivo, *J. Bone Miner. Res.*, 2011, **26**(11), 2634–2646.
- 59 J. S. Wang, C. M. Mazur and M. N. Wein, Sclerostin and Osteocalcin: Candidate Bone-Produced Hormones. Frontiers in, *Endocrinology*, 2021, **12**, 584147.
- 60 A. G. Robling and L. F. Bonewald, The Osteocyte: New Insights, *Ann. Rev. Physiol.*, 2020, **82**, 485–506.
- 61 R. Owen, *et al.*,  $\beta$ -glycerophosphate, not low magnitude fluid shear stress, increases osteocytogenesis in the



- osteoblast-to-osteocyte cell line IDG-SW3, *Connect. Tissue Res.*, 2024, 1–17.
- 62 L. F. Bonewald, Establishment and characterization of an osteocyte-like cell line, MLO-Y4, *J. Bone Miner. Metab.*, 1999, 17(1), 61–65.
- 63 M. Prideaux, *et al.*, Generation of two multipotent mesenchymal progenitor cell lines capable of osteogenic, mature osteocyte, adipogenic, and chondrogenic differentiation, *Sci. Rep.*, 2021, 11(1), 22593.
- 64 J. Kim and T. Adachi, Cell-fate decision of mesenchymal stem cells toward osteocyte differentiation is committed by spheroid culture, *Sci. Rep.*, 2021, 11(1), 13204.
- 65 H. J. Knowles, *et al.*, Mature primary human osteocytes in mini organotypic cultures secrete FGF23 and PTH1-34-regulated sclerostin, *Front. Endocrinol.*, 2023, 14, 1167734.
- 66 A. Iordachescu, *et al.*, Trabecular bone organoids: a micron-scale ‘humanised’ prototype designed to study the effects of microgravity and degeneration, *npj Microgravity*, 2021, 7(1), 17.
- 67 M. Koide, *et al.*, Sclerostin expression in trabecular bone is downregulated by osteoclasts, *Sci. Rep.*, 2020, 10(1), 13751.
- 68 M. Zhu, *et al.*, Sclerostin induced tumor growth, bone metastasis and osteolysis in breast cancer, *Sci. Rep.*, 2017, 7(1), 11399.
- 69 M. Pereira, *et al.*, Sclerostin does not play a major role in the pathogenesis of skeletal complications in type 2 diabetes mellitus, *Osteoporosis Int.*, 2017, 28(1), 309–320.
- 70 M. H. Amer, L. J. White and K. M. Shakesheff, The effect of injection using narrow-bore needles on mammalian cells: administration and formulation considerations for cell therapies, *J. Pharm. Pharmacol.*, 2015, 67(5), 640–650.
- 71 N. Mangir, *et al.*, Using ex Ovo Chick Chorioallantoic Membrane (CAM) Assay To Evaluate the Biocompatibility and Angiogenic Response to Biomaterials, *ACS Biomater. Sci. Eng.*, 2019, 5(7), 3190–3200.
- 72 R. Schneider-Stock and G. Flügen, Editorial for Special Issue: The Chorioallantoic Membrane (CAM) Model--Traditional and State-of-the Art Applications: The 1st International CAM Conference, *Cancers*, 2023, 15(3), 772.
- 73 B. L. Krock, N. Skuli and M. C. Simon, Hypoxia-induced angiogenesis: good and evil, *Genes Cancer*, 2011, 2(12), 1117–1133.
- 74 C. A. Schneider, W. S. Rasband and K. W. Eliceiri, NIH Image to ImageJ: 25 years of image analysis, *Nat. Methods*, 2012, 9(7), 671–675.
- 75 D. R. Stirling, *et al.*, CellProfiler 4: improvements in speed, utility and usability, *BMC Bioinf.*, 2021, 22(1), 433.
- 76 J. Misra, *et al.*, Zoledronate Attenuates Accumulation of DNA Damage in Mesenchymal Stem Cells and Protects Their Function, *Stem Cells*, 2016, 34(3), 756–767.
- 77 G. Gigliobianco, C. K. Chong and S. MacNeil, Simple surface coating of electrospun poly-L-lactic acid scaffolds to induce angiogenesis, *J. Biomater. Appl.*, 2015, 30(1), 50–60.

